Cloud Physics Lidar: instrument description and initial measurement results

Matthew McGill, Dennis Hlavka, William Hart, V. Stanley Scott, James Spinhirne, and Beat Schmid

The new Cloud Physics Lidar (CPL) has been built for use on the NASA ER-2 high-altitude aircraft. The purpose of the CPL is to provide multiwavelength measurements of cirrus, subvisual cirrus, and aerosols with high temporal and spatial resolution. The CPL utilizes state-of-the-art technology with a high repetition rate, a low-pulse-energy laser, and photon-counting detection. The first deployment for the CPL was the Southern African Regional Science Initiative's 2000 field campaign during August and September 2000. We provide here an overview of the instrument and initial data results to illustrate the measurement capability of the CPL. © 2002 Optical Society of America

OCIS codes: 010.1100, 010.3640, 280.0280, 280.3640.

1. Introduction

The effect of clouds and aerosols on regional and global climate is of great importance. An important element of the NASA climate and radiation science program is field studies that incorporate airborne remote sensing and *in situ* measurements of clouds and aerosols. These field experiments involve coordination of ground-based and satellite measurements with the airborne observations. The goals of such experiments include testing satellite remote-sensing retrievals, developing advanced remote-sensing techniques, and providing fundamental advances in knowledge of cloud radiation and microphysical properties.

One of the most important components of airborne remote-sensing experiments is the high-altitude NASA ER-2 aircraft. Because the ER-2 typically flies at approximately 65,000 ft (20 km), its instruments are above 94% of the Earth's atmosphere, thereby allowing ER-2 instruments to function as spaceborne instrument simulators. The ER-2 provides a unique platform for atmospheric profiling, particularly for active remote sensing instruments such as lidar. A typical ER-2 remote-sensing experiment combines multispectral passive cloud remote sensing with active lidar or radar profiling or both. A key application is testing of cloud remote sensing algorithms and verification of satellite measurements. In these situations, active lidar profiling is especially valuable because the cloud height structure, up to the limit of signal attenuation, is unambiguously measured.

The Cloud Lidar System (CLS) was the first high-altitude lidar system designed specifically for studying clouds and aerosols[1–3] and was first flown on the ER-2 aircraft in 1983. In subsequent years the CLS was modified as necessary to stay current with improving technology. The CLS participated in a large number of major field campaigns including the Tropical Ocean Global Atmosphere–Coupled Ocean-Atmosphere Response Experiment (TOGA–COARE), the Central Equatorial Pacific Experiment (CEPEX), the First ISCCP Regional Experiment (FIRE), and the Subsonic Aircraft: Contrail and Cloud Effects Special Study (SUCCESS).[4–8] The CLS historically provided basic lidar cloud and aerosol observations at 1064 and 532 nm. Standard CLS data products included cloud boundary altitudes and vertical profiles of cloud and aerosol structure, up to the limit of signal attenuation.

The CLS data have been applied in studies involving retrieval of cloud microphysical parameters. The visible optical thickness for transmissive clouds can, in principal, be obtained from the decrease in

M. McGill (mcgill@virl.gsfc.nasa.gov), V. S. Scott, and J. Spinhirne are with the NASA Goddard Space Flight Center, Code 912, Greenbelt, Maryland 20771. D. Hlavka and W. Hart are with Science Systems and Applications, Incorporated, 5900 Princess Garden Parkway, Suite 300, Lanham, Maryland 20706. B. Schmid is with the Bay Area Environmental Research Institute, 645 Anthony Court, Sonoma, California 95476.

Received 8 October 2001; revised manuscript received 28 February 2002.

0003-6935/02/183725-10$15.00/0

signals beyond the lower cloud boundary,[3] but both multiple scattering and practical limitations of the analog signal acquisition of the CLS introduce significant uncertainties. Such limitations eventually led investigators to consider a new version of CLS that would be designed to alleviate the difficulties inherent in the CLS hardware and the growing difficulties owing to age (e.g., spare parts). That, coupled with increasing desires for enhanced science capabilities, strongly suggested the need for a new instrument. Ultimately, a decision was made to develop an entirely new instrument to replace the CLS. The new instrument would have increased science capabilities, a smaller size, and a reduced mass and would utilize newer component technologies.

2. Cloud Physics Lidar

In designing the Cloud Physics Lidar (CPL), three primary considerations drove the instrument design: (1) make the system eye safe at the operating altitude; (2) make the system as lightweight as possible, yet rugged; and (3) use solid-state photon-counting detectors. In addition, all mechanical and safety considerations relating to the ER-2 aircraft had to be accommodated. Although primarily intended for use on the ER-2, the CPL is designed to also fit other aircraft such as the WB-57 and potentially even unmanned aircraft.

In recent years there have been significant advances in the approach to lidar design. A now-proven approach is to use a high repetition rate laser, operating at multiple kHz rather than tens of Hz, but at low pulse energies. Ground-based systems of this type, such as the micropulse lidar,[9,10] have been in use since the early 1990's. Advantages of using a high-repetition-rate laser are the potential of eye safety from low pulse energies, a more compact size, a greater reliability, and turnkey ease of use. A basic requirement of using a high-repetition-rate laser is a narrow field of view, along with narrow-band filtering, to minimize solar background noise. An added advantage is that the field of view is small enough to essentially eliminate multiple-scattered signal.

Because the pulse energy is low, the instrument can be designed to use photon-counting detection. Solid-state photon-counting detectors are readily available and have good quantum efficiencies with low thermal noise. More important, the photon-counting detectors permit easy data inversion without the need for complicated calibration schemes or calibration of log-amplifiers, as is needed when analog detectors are used. The disadvantage of photon-counting detectors is their inherently small dynamic range. However, the use of photon-counting detectors along with high-repetition-rate lasers still allows for wide dynamic range in the measured signal; the dynamic range is attained by accumulation over many pulses.

Science goals immediately dictated that the system be designed around a three-wavelength laser. The laser transmitter is a solid-state, conductively cooled system made by LiteCyles, Inc. (2301 North Forbes Boulevard, Suite 111, Tucson, Arizona 85745). The laser is a neodymium vanadate ($Nd:YVO_4$) oscillator with doubling and tripling crystals generating 1064-, 532-, and 355-nm outputs simultaneously and collinear. The laser head is housed in the instrument box and is fiber optically coupled to the power supply and diodes. The pump diodes are located outside the instrument box to aid in dissipating the heat generated by the diodes and associated electronics. Output energies at each wavelength are given in Table 1.

Table 1. CPL System Parameters

Parameter	Value
Wavelengths	1064, 532, and 355 nm
Laser type	Solid-state $Nd:YVO_4$
Laser repetition rate	5 kHz
Laser output energy	50 μJ at 1064 nm 25 μJ at 532 nm 50 μJ at 355 nm
Telescope diameter	20 cm
Telescope type	Off-axis parabola
Telescope field of view	100 μrad, full angle
Effective filter bandwidth (full width, half-height)	240 pm at 1064 nm 120 pm at 532 nm 150 pm at 355 nm
Filter efficiency	81% at 1064 nm 60% at 532 nm 45% at 355 nm
Detector efficiency (all detectors fiber coupled)	3% at 1064 nm 60% at 532 nm 10% at 355 nm
Raw data resolution	1/10 s (30 m vertical by 20 m horizontal)
Processed data resolution	1 s (30 m vertical by 200 m horizontal)

The telescope is used as part of the beam expander, similar to MicroPulse Lidars. However, unlike MicroPulse Lidars, the CPL utilizes a 20-cm-diameter off-axis parabola as the telescope primary. The off-axis parabola not only permits a rugged and robust design but also eliminates most obscurations to both the outgoing and the incoming beams. In fact, none of the outgoing light is lost to obscurations, and only approximately 20% of the receiver aperture is obscured. The return signal collected by the telescope is separated into wavelength components by use of dichroics. The 1064-nm return is further separated into parallel- and perpendicular-polarization components. Once the wavelengths are separated, each component is passed through a narrow-band interference filter(s) and fiber optically coupled to an appropriate detector. For the 532- and 1064-nm channels a pair of matched interference filters is used to provide better solar rejection. A half-wave plate is located in the 1064-nm path to allow calibration of the parallel and perpendicular channels. A simplified schematic diagram of the CPL optics is shown in Fig. 1.

An important feature of the CPL is the integrating

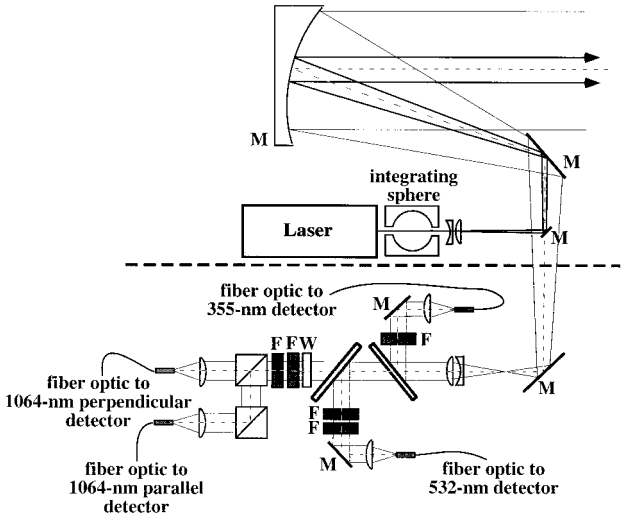

Fig. 1. Simplified optical diagram of CPL (not to scale). Components are labeled as follows: F, interference filters; M, mirrors; and W, half-wave plate. Components lying above the dashed line are mounted on one side of the optical breadboard, and components lying below the dashed line are mounted on the opposite side.

sphere located at the laser output. The integrating sphere collects light scattered from lenses that follow it. There are three energy monitor detectors located at ports in the integrating sphere. Each detector has appropriate filtering such that the laser output energy is measured independently for each wavelength. The laser output energy is measured on each pulse to permit the most accurate calibration possible.

As mentioned previously, the overall instrument design was driven by a desire to use simple photon-counting detectors. The 1064-nm detectors are single-photon-counting modules. These detectors have approximately 3% quantum efficiency and low thermal noise (less than 200 counts/s). The 532-nm channel also utilizes single-photon-counting modules, the quantum efficiency being approximately 60% at that wavelength. The 355-nm channel uses a photon-counting photomultiplier tube to allow for good quantum efficiency (~20%) and larger dynamic range for the enhanced Rayleigh signal. Output from the detectors are counted by a multichannel range-gating card made by ASRC Aerospace Corporation (6301 Ivy Lane, Suite 300, Greenbelt, Maryland 20770).

The laser head and transmit optics are mounted on one side of an optical breadboard. The receiver optics are mounted on the back side of the same breadboard. The optical breadboard is housed in a sealed box to maintain a clean, thermally stable, and dry environment. For vibration isolation the breadboard mounts to the box via a three-point kinematic mounting system. Figure 2 shows front and back views of the optical breadboard with all components mounted. The breadboard is compact to fit within the ER-2 and measures only 55 cm × 30 cm.

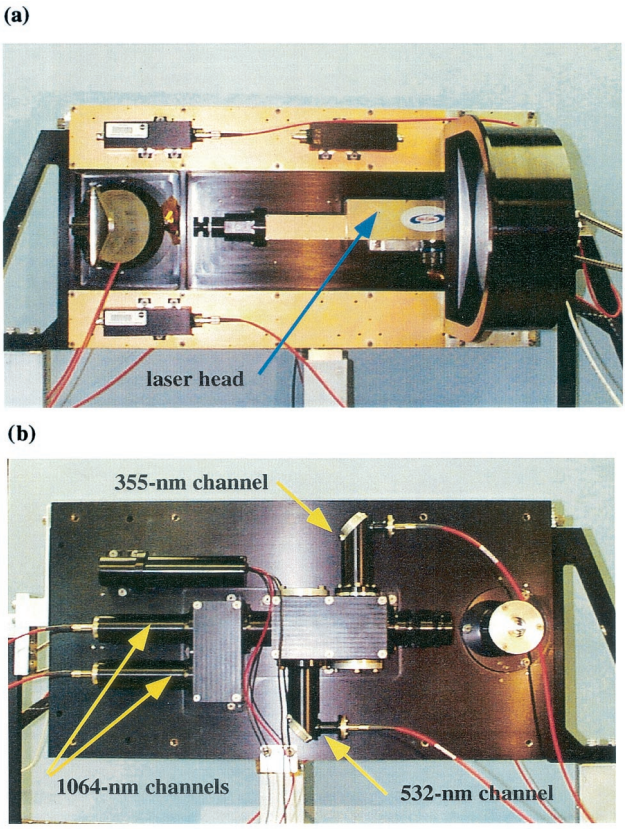

Fig. 2. (a) Photo of the transmitter side of the optical breadboard, showing the laser head and off-axis mirror. (b) Photo of the receiver side of the optical breadboard, showing the component layout and the different wavelength channels.

3. Science Capabilities of the Cloud Physics Lidar

The CPL provides a complete ensemble of cloud physics information. Primary data products include

- Cloud profiling with 30-m vertical and 200-m horizontal resolution at 1064, 532, and 355 nm, providing cloud location and an internal backscatter structure.
- Aerosol, boundary layer, and smoke plume profiling at all three wavelengths, providing calibrated profiles of backscatter coefficients.
- Depolarization ratio to determine the phase (e.g., ice or water) of clouds by use of the 1064-nm output.
- Cloud particle size determined from comparison of backscatter at the three wavelengths.
- Determination of optical depth for both cloud and aerosol layers (up to the limit of signal attenuation, ~optical depth of 3).
- Direct determination of the optical depth of cirrus clouds (up to ~optical depth of 3) by use of the 355-nm output.
- Determination of the extinction-to-backscatter parameter.

The CPL provides information to permit a comprehensive analysis of radiative and optical properties of

optically thin clouds. To determine the effects of particulate layers on the radiative budget of the Earth–atmosphere system, certain information about the details of the layer and its constituents is required. The effect of cirrus clouds on the Earth's radiation budget has long been recognized.[11] The interaction of radiation with cirrus clouds, termed cloud radiative forcing, is important for both regional- and global-scale energy budgets. The information required to compute the radiative forcing includes the vertical distribution of a short-wave cross section, a parameter that the CPL can provide, up to the limit of optical signal attenuation.

By use of optical depth measurements determined from attenuation of Rayleigh and particulate scattering and by use of the integrated backscatter, the extinction-to-backscatter parameter can be derived under favorable atmospheric conditions. This permits rapid analysis of cloud optical depth because only lidar data are required; there is no need to use other instrumentation.[3] By use of the derived extinction-to-backscatter ratio, the internal cloud extinction profile can then be obtained.

The CPL uses photon-counting detectors with a high repetition rate laser to maintain a large signal dynamic range. This dramatically reduces the time required to produce reliable and complete data sets. The goal of the CPL analysis is to provide, within 24 h of a flight, data including (1) cloud and aerosol quicklook pictures, (2) cloud and aerosol layer boundaries, and (3) depolarization information. The optical depth determinations require more careful analysis. Determination of optical depths for uncomplicated layers of cirrus clouds with homogeneous scattering characteristics can be completed within a day by use of an automated analysis algorithm. However, situations in which the cloud layering and structure are complex, which often preclude an automated data-processing algorithm, may require several weeks for processing.

Multiply scattered signal is a known problem for cloud and aerosol remote sensing by conventional lidar. For a standard lidar equation, it is generally assumed that only first-order scattering is collected by the receiver. However, most lidar systems have wide receiver fields of view that necessarily collect multiply scattered signal when a dense medium (e.g., cloud) is encountered. When multiply scattered signal is present but not accounted for in data analysis, incorrect estimates of the extinction-to-backscatter parameter and optical depth can occur. Multiple scattering is difficult to predict owing to the dependence on both the measurement geometry and the particle size. The CLS receiver had a field of view of 1.6-mrad full angle. When dense media were encountered, the multiply scattered contribution was significant. For CLS retrievals, the correction to direct optical thickness was approximately a factor of two but could vary by more than 50%.[12] The new CPL receiver has a field of view of only a 100-μrad full angle. Although not entirely eliminating multiply scattered signals, the small field of view does greatly minimize collection of multiply scattered signals. Simulations show that the amount of multiple-scattered signal should be 5% or less of the total measured signal for thin cirrus and no more than 15% for clouds of optical depth of 2.

4. First Flights and Sample Data

The first field deployment for the CPL was the Southern African Regional Science Initiative (SAFARI) campaign in southern Africa during August and September 2000.[13,14] The purpose of SAFARI was to study the unique climatology of southern Africa, with particular emphasis on biomass burning and other regional emissions. During the SAFARI campaign, the CPL provided data on cloud height and structure as well as aerosol and smoke plume structure. The goal is to use CPL data to determine quantitative optical characteristics of both clouds and smoke layers. The CPL data will be used in conjunction with other airborne and ground-based instrumentation, as well as satellite data, to quantify and validate the regional emissions. Data from the SAFARI campaign will be used to understand the linkages between land–atmosphere processes. Although detailed analysis of data will be the focus of future papers, we present here some initial results to demonstrate the data collection capability of the CPL.

As with any lidar, instrument corrections (e.g., overlap and detector dead time) must be applied, and the system must be calibrated before data products can be retrieved. For the CPL we have developed a standardized calibration routine. The most important part of the calibration is knowing how much energy is transmitted to the atmosphere for each measurement. To measure the output energy of the laser, we use an energy monitor detector (a photodiode) to sample the laser output. Separate detectors are used for each wavelength, thus ensuring that each wavelength can be independently and accurately calibrated. The energy monitor detector is calibrated to the laser energy in a laboratory setting. This calibration provides a relationship between laser energy and energy-monitor output that is used to energy normalize the CPL measurements during operation. During operation the energy monitors sample the laser energy on every pulse to ensure that an accurate measure of the output energy is obtained. To obtain the instrument calibration constant, we adjust the measured, energy-normalized CPL profile to match a molecular profile at high altitude. The molecular profile is obtained through either standard atmosphere models or, if available, balloon soundings or other local sources of temperature–pressure profiles. In the data-processing stage, the instrument calibration is calculated for every profile and then averaged over 5-min intervals.

During the SAFARI campaign the CPL instrument operated properly, and good data from the 532- and 1064-nm channels were obtained. A custom optic for the 355-nm channel was not delivered in time, which precluded use of that channel for the SAFARI mission. During the SAFARI mission, 120 flight

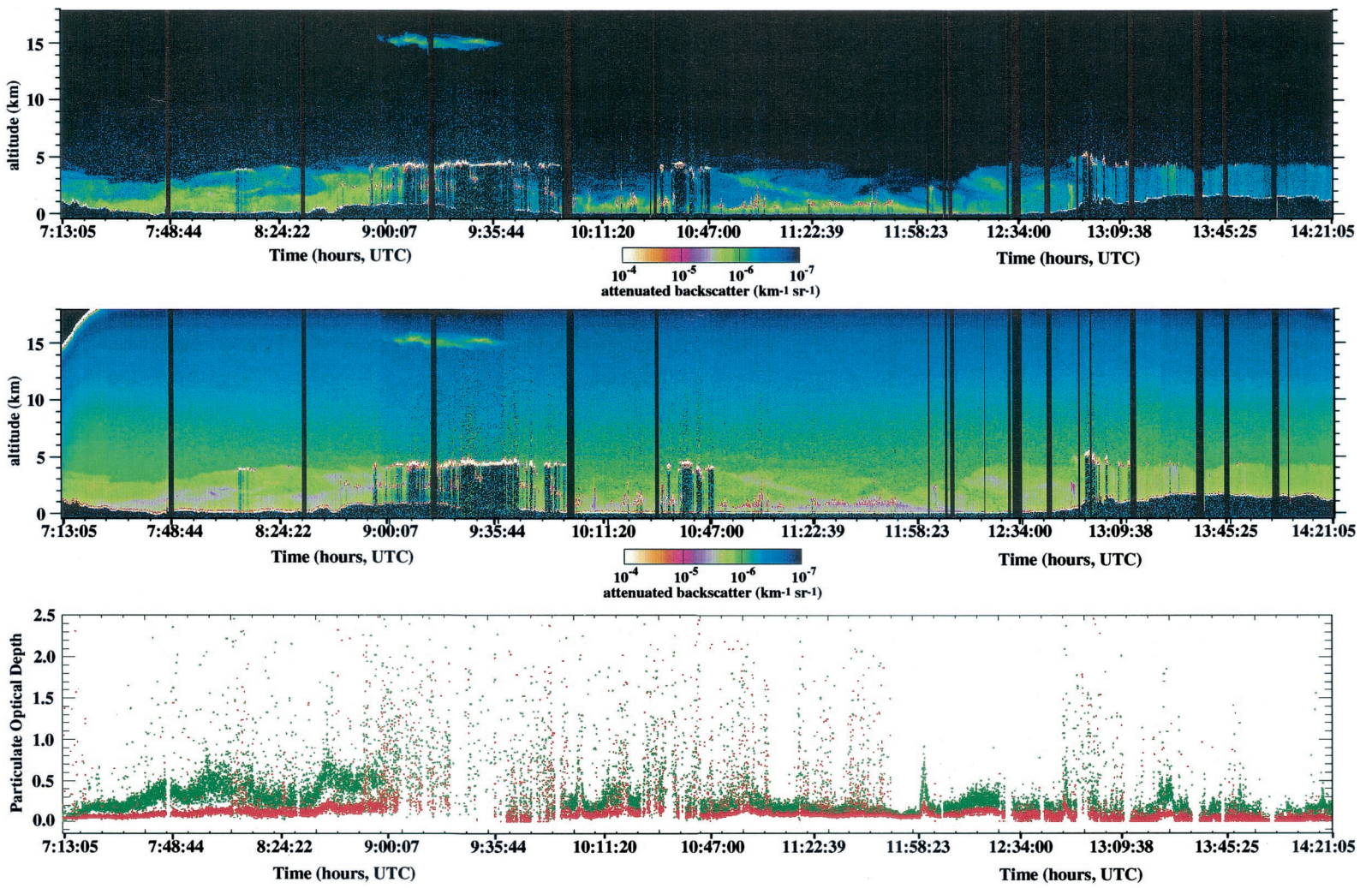

Fig. 3. CPL data from 25 September, 2000. Top panel, 1064-nm attenuated backscatter profiles. Middle panel, 532-nm attenuated backscatter profiles. Bottom panel, the derived total optical depth. The green trace is the 532-nm optical depth, and the red trace is 1064 nm. The plot shows the entire flight, illustrating the variability and structure that can be seen in the lidar data. Dense clouds are bright white, and cloud shadows are present whenever the lidar signal cannot penetrate through a layer.

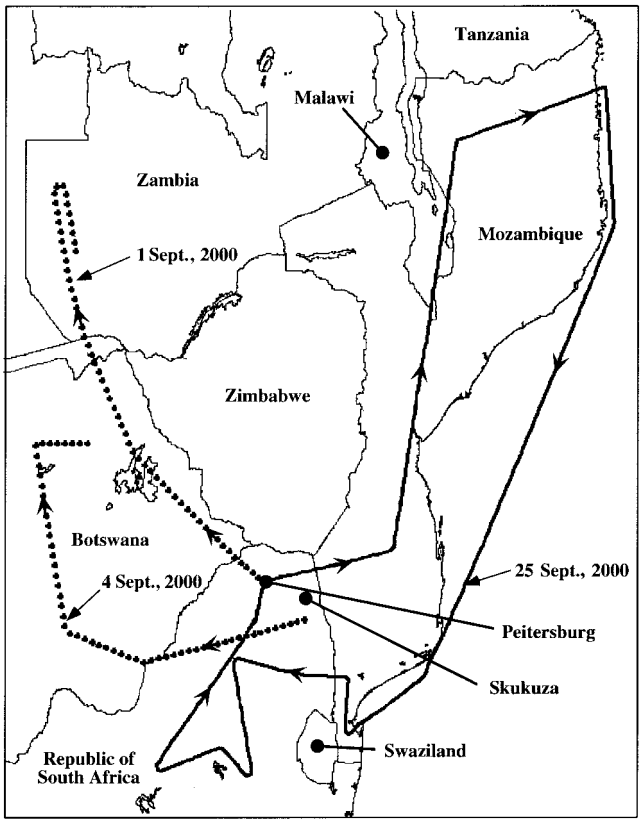

Fig. 4. ER-2 flight tracks for 1, 4, and 25 September, 2000.

hours of data were obtained by CPL with no problems or failures. Figure 3 shows a plot of attenuated backscatter over the course of an entire flight on 25 September, 2000. The top panel is the 1064-nm attenuated backscatter (sum of both parallel and perpendicular channels), and the middle panel is the 532-nm attenuated backscatter. The bottom panel in Fig. 3 is the derived total particulate optical depth by wavelength. As evidenced in Fig. 3, the signal-to-noise ratios in both the 1064- and the 532-nm data are extremely good. At higher altitudes the 1064 profiles reflect the absence of both aerosol and molecular scatterers at high altitudes. The standard deviation of the total particulate optical depth, calculated by averaging over periods in which clouds are not present and natural variability is minimal, varies from 0.04–0.08 for 532 nm and 0.02–0.03 for 1064 nm. To aid in interpreting the data, we present in Fig. 4 the flight tracks for all data segments used in this paper.

During the SAFARI campaign there was only one flight that encountered any significant cirrus clouds. A 2-h segment of data from 4 September, 2000 is shown in Fig. 5. The top panel shows the 532-nm attenuated backscatter, and the bottom panel shows the retrieved cirrus optical depth by wavelength. For this data segment, the extinction-to-backscatter ratio (S ratio) was preset to 29.5 sr for both the 532- and the 1064-nm channels if the ratio could not be calculated. The retrieved cirrus optical depth exhibits no wavelength dependence. This result verifies proper behavior of the optical depth retrieval algorithm, because cirrus clouds are expected to be "white" scatterers (e.g., all wavelengths are scattered equally).

Of particular interest in the SAFARI campaign were optical properties of the planetary boundary layer (PBL) that were due to smoke from extensive biomass burning. Figure 6 shows a 2-h segment of data from 1 September, 2000. The top panel is the 1064-nm total backscatter showing the structure of aerosols within the boundary layer. The boundary layer is capped by a strong inversion, with little aerosol above the capping level. The bottom panel in Fig. 6 is the aerosol optical depth by wavelength for the boundary layer, calculated from the top of the layer down to the ground. Two features are evident in the data. First, the optical depth of the boundary layer increases as the flight proceeds. Second, there is a strong wavelength dependence presumably caused by large concentrations of smoke particles. In fact, in the latter half of the data segment the optical depth becomes large enough that the 532-nm lidar signal is almost fully attenuated before reaching the ground, thereby resulting in noisy 532-nm retrievals. For processing this data segment, the extinction-to-backscatter ratio (S ratio) was fixed at 57 sr for the 532 nm and 49 sr for the 1064 nm. These S-ratio values are consistent with a smoke-polluted boundary layer.[15]

As part of the SAFARI field campaign, ground-based MicroPulse Lidar systems were deployed at two field locations. One system was located in the Skukuza National Park in South Africa, and the other was in Mongu, Zambia. At several times during the campaign, the ER-2 was directed to overfly the MicroPulse Lidar sites to allow calibration and comparison of the ground-based and airborne sensors. Figure 7 shows one such comparison of extinction profiles derived from the CPL and MicroPulse Lidar on 22 August, 2000. In this particular case, the ER-2 flew no closer than 5 miles to the MicroPulse Lidar site. This difference in exact location probably accounts for differences between the profiles in the lowest kilometer. In this example the CPL profile is a 30-s average, whereas the MicroPulse Lidar profile is a 30-min average. For the calculation of the extinction profiles, the extinction-to-backscatter ratio (S ratio) for the 532-nm channel was fixed at 61 sr, and the MicroPulse Lidar (operating at 523 nm) S ratio was fixed at 74 sr. Both lidars used Aerosol Robotic Network (AERONET) Cimel[16] optical depth measurements colocated at the MicroPulse Lidar site to calculate the S ratios.

Also participating in the SAFARI campaign was the NASA Ames airborne tracking 14-channel sunphotometer (AATS-14) onboard the University of Washington CV-580 aircraft. The AATS-14 measures atmospheric transmission (and hence optical depth and extinction) in bands from 354 to 1558 nm.[17] The channels of interest to CPL are those at 525 and 1020 nm, close to the CPL wavelengths. The

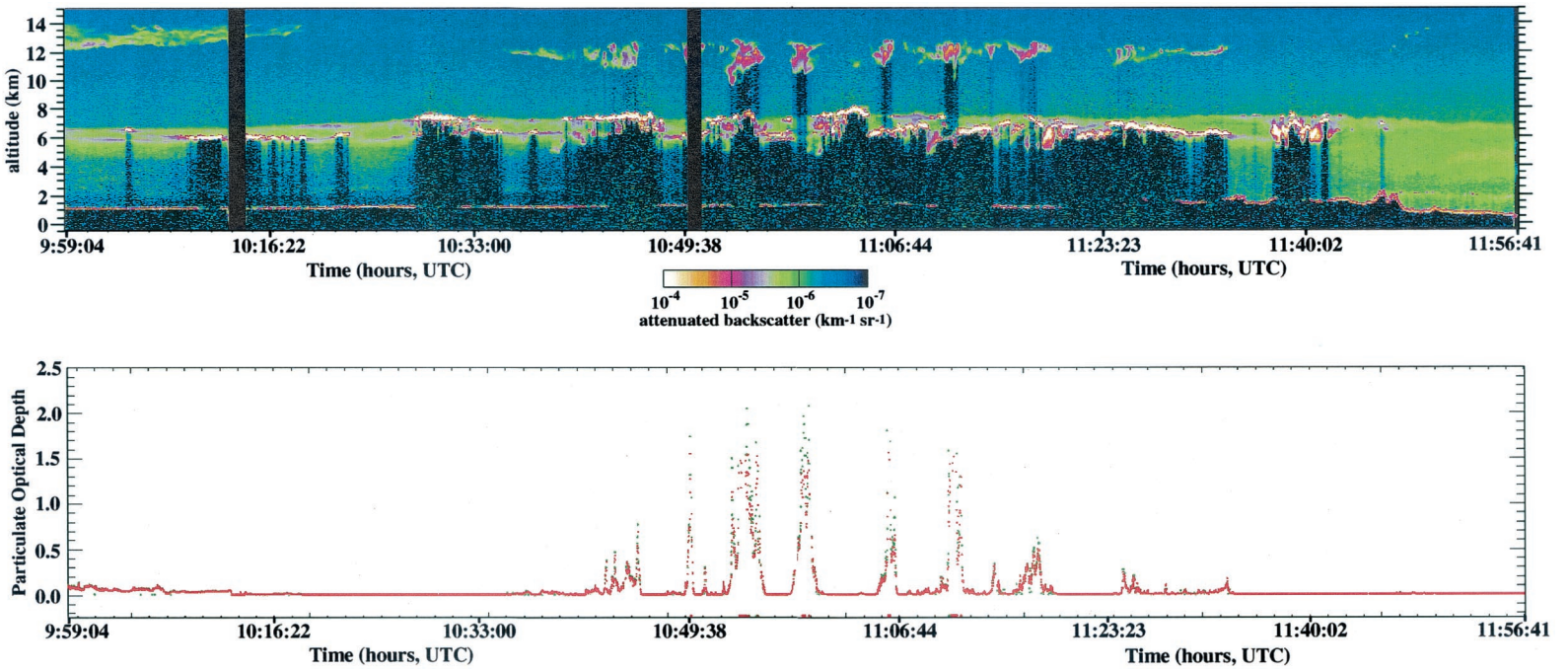

Fig. 5. Cirrus optical depth from 4 September, 2000. Plot shows 2 h of data. Top panel, the 532-nm attenuated backscatter coefficient. Bottom panel, the retrieved cirrus optical depth. The cirrus optical depth is the optical depth that is due to particulates in the 9–15-km region. In the bottom panel, the green trace is the 532-nm optical depth, and the red trace is the 1064-nm optical depth. As expected, there is no wavelength dependence on the cirrus optical depth.

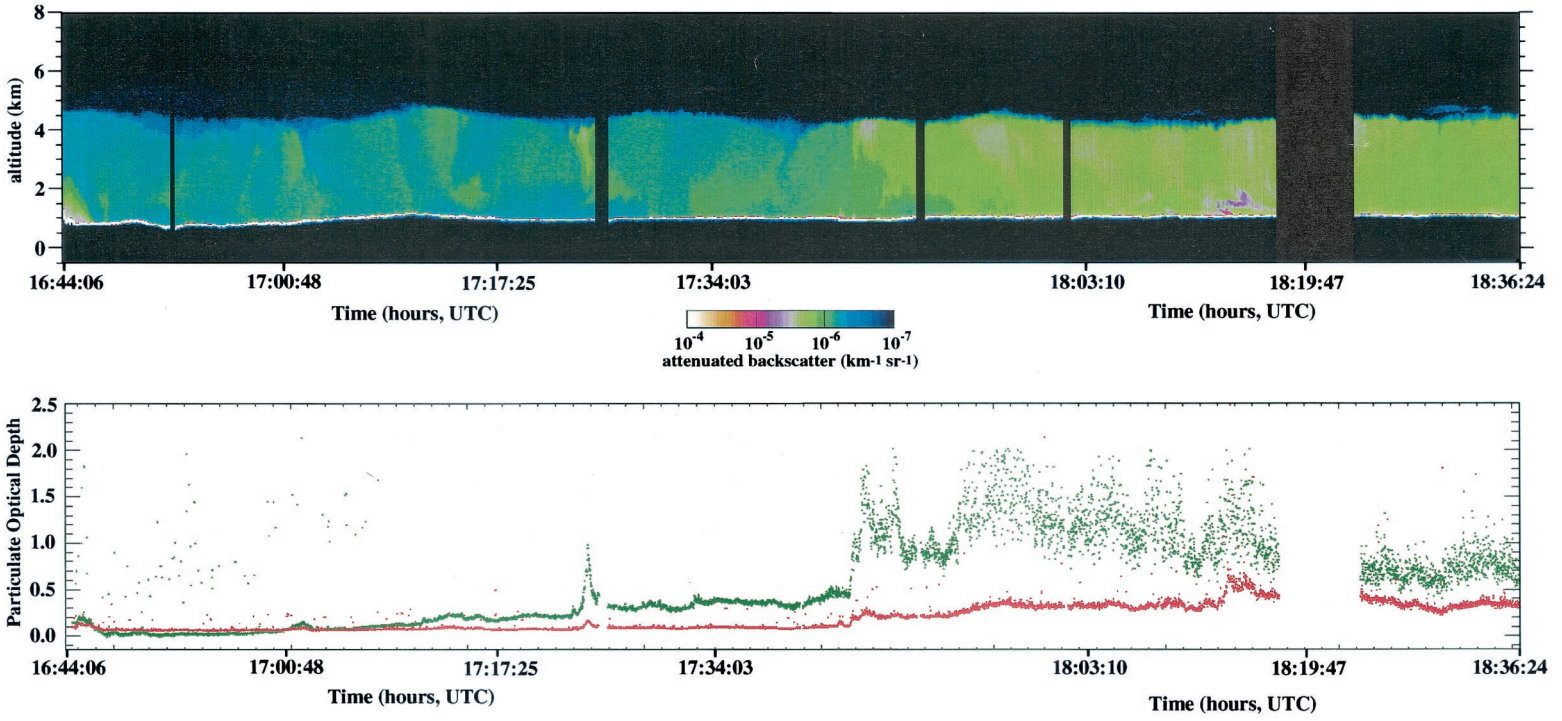

Fig. 6. PBL optical depth from 1 September 2000. Plot shows 2 h of data. Top panel, the 1064-nm attenuated backscatter coefficient. Bottom panel, the resultant aerosol optical depth for the PBL only. In the bottom panel, the green trace is the 532-nm optical depth, and the red trace is the 1064-nm optical depth. Evidently, there is a strong wavelength dependence that is due to heavy smoke in the PBL. At some points the 532-nm attenuation becomes so great that the optical depth becomes noisy.

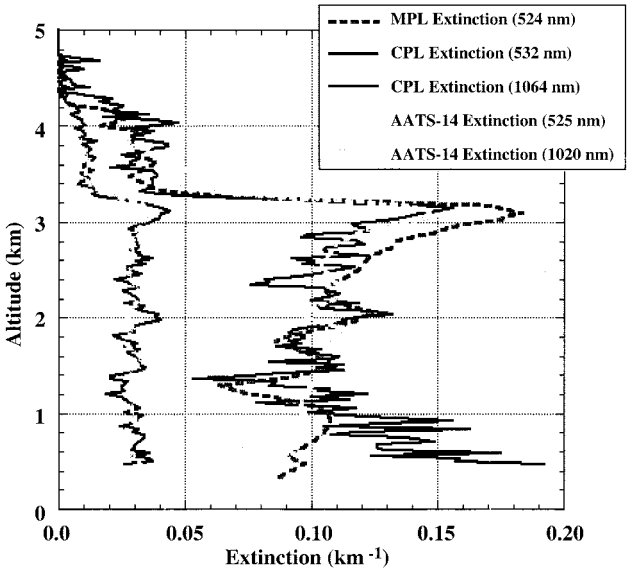

Fig. 7. Comparison of extinction profiles from CPL, micropulse lidar (MPL) and the Ames airborne tracking 14-channel sunphotomer (AATS-14) for 22 August 2000. The MPL was sited at Skukuza, and the AATS-14 was onboard the CV-580 aircraft. On that day the ER-2 flew within 5 miles of the MPL site, as did the CV-580. Despite slight wavelength differences among the three instruments, there is good agreement in the retrieved extinction profiles. The MPL profile is a 30-min average, and the CPL profile is a 30-s average.

AATS-14 extinction profiles are overplotted in Fig. 7. The agreement with the CPL 1064-nm profile is quite good. At the shorter 532-nm wavelength the agreement is also good, although, as expected, there is greater wavelength dependence owing to the differences in operating wavelength among the three instruments. Nonetheless, this result indicates that the CPL instrument and analysis algorithms do provide accurate measurements of aerosol optical properties.

5. Conclusion

During 1999 and 2000 a new cloud and aerosol lidar system, the Cloud Physics Lidar, was built for use on the high-altitude NASA ER-2 aircraft. The CPL provides measurements at three wavelengths to permit a comprehensive study of cloud and aerosol properties. The CPL is designed around a high repetition rate and a low pulse energy laser transmitter. Photon-counting detection is used to simplify the data inversion process. Although photon-counting detectors have limited bandwidth, use of the high repetition rate laser allows for large dynamic range through pulse accumulation at low pulse energy.

The first field deployment for the CPL was the SAFARI 2000 campaign during August and September 2000. During the SAFARI mission the CPL provided measurements of boundary layer structure and optical properties to aid in studies of biomass burning. Examples have been shown to illustrate the data collection capability of the CPL. It is demonstrated that aerosol variability and structure are measured during daylight conditions. Retrieved optical depth estimates are consistent with expectations. Comparisons of CPL-derived extinction profiles compare favorably with those from other lidar and *in situ* instruments.

The cloud physics lidar is sponsored by NASA's Earth Observing System office and by NASA Radiation Sciences, Code YS. We thank Ellsworth Welton of Goddard Earth Science and Technology Center for providing the MicroPulse Lidar data and Brent Holben of Aerosol Robotic Network for Skukuza Cimel data. Data presented in this paper were collected during the Southern African Regional Science Initiative (SAFARI-2000).

References

1. J. D. Spinhirne, M. Z. Hansen, and L. O. Caudill, "Cloud top remote sensing by airborne lidar," Appl. Opt. **21,** 1564–1571 (1982).
2. J. D. Spinhirne, M. Z. Hansen, and J. Simpson, "The structure and phase of cloud tops as observed by polarization lidar," J. Appl. Meteorol. **22,** 1319–1331 (1983).
3. J. D. Spinhirne and W. D. Hart, "Cirrus structure and radiative parameters from airborne lidar and spectral radiometer observations: the 28 October 1986 FIRE study," Mon. Weather Rev. **118,** 2329–2343 (1990).
4. J. D. Spinhirne, W. D. Hart, and D. L. Hlavka, "Cirrus infrared parameters and shortwave reflectance relations from observations," J. Atmos. Sci. **53,** 1438–1458 (1996).
5. D. P. Duda, J. D. Spinhirne, and W. D. Hart, "Retrieval of contrail microphysical properties during SUCCESS by the split-window method," Geophys. Res. Lett. **25,** 1149–1152 (1998).
6. J. D. Spinhirne, W. D. Hart, and D. Duda, "Evolution of the morphology and microphysics of contrail cirrus from airborne active and passive remote sensing," Geophys. Res. Lett. **23,** 1153–1156 (1998).
7. J. R. Wang, P. Racette, J. D. Spinhirne, K. F. Evans, and W. D. Hart, "Observations of cirrus clouds with airborne MIR, CLS, and MAS during SUCCESS," Geophys. Res. Lett. **25,** 1145–1148 (1998).
8. A. J. Heymsfield, G. M. McFarquhar, W. D. Collins, J. A. Goldstein, F. P. J. Valero, J. Spinhirne, W. Hart, and P. Pilewskie, "Cloud properties leading to highly reflective tropical cirrus: interpretations from CEPEX, TOGA COARE, and Kwajalein, Marshall Islands," J. Geophys. Res. [Atmos] **103,** 8805–8812 (1998).
9. J. D. Spinhirne, "Micro pulse lidar," IEEE Trans. Geosci. Remote Sens. **31,** 48–55 (1993).
10. J. D. Spinhirne, J. A. R. Rall, and V. S. Scott, "Compact eye safe lidar systems," Rev. Laser Eng. **23,** 112–118 (1995).
11. Y. J. Kaufman, P. V. Hobbs, V. W. J. H. Kirchoff, P. Artaxo, L. A. Remer, B. N. Holben, M. D. King, D. E. Ward, E. M. Prins, K. M. Longo, L. F. Mattos, C. A. Nobre, J. D. Spinhirne, Q. Ji, A. M. Thompson, J. F. Gleason, S. A. Christopher, and S. C. Tsay, "Smoke, clouds, and radiation—Brazil (SCAR-B) experiment," J. Geophys. Res. [Atmos] **103,** 31783–31808 (1998).
12. C. M. R. Platt, J. D. Spinhirne, and W. D. Hart, "Optical and microphysical properties of a cold cirrus cloud: evidence for regions of small ice particles," J. Geophys. Res. **94,** 11151–11164 (1989).
13. R. J. Swap and J. Privette, "Overview of the southern African regional science initiative—SAFARI 2000," in *Proceedings of IEEE 1999 International Geoscience and Remote Sensing Sym-*

posium (Institute of Electrical and Electronics Engineers, New York, 1999), pp. 595–597.
14. B. Swap, J. Privette, M. King, D. Starr, T. Suttles, H. Annegarn, M. Scholes, and C. O. Justice, "SAFARI 2000: a southern African regional science initiative," EOS Earth Observer, **10,** 25–28 (1998).
15. J. Ackerman, "The extinction-to-backscatter ratio of tropospheric aerosol: a numerical study," J. Atmos. Ocean. Technol. **15,** 1043–1050 (1998).
16. B. N. Holben, T. F. Eck, I. Slutsker, D. Tanre, J. P. Buis, A. Setzer, E. Vermote, J. A. Reagan, Y. J. Kaufman, T. Nakajima, F. Lavenu, I. Jankowiak, and A. Smirnov, "AERONET—a federated instrument network and data archive for aerosol characterization," Remote Sensing Environ. **66,** 1–16 (1998).
17. B. Schmid, J. M. Livingston, P. B. Russell, P. A. Durkee, H. H. Jonsson, D. R. Collins, R. C. Flagan, J. H. Seinfeld, S. Gasso, D. A. Hegg, E. Ostrom, K. J. Noone, E. J. Welton, K. J. Voss, H. R. Gordon, P. Formenti, and M. O. Andreae, "Clear-sky studies of lower tropospheric aerosol and water vapor during ACE-2 using airborne sunphotomoeter, airborne in-situ, space-borne, and ground-based measurements," Tellus B **52,** 568–593 (2000).